[Article] DOI: 10.13208/j.electrochem.2219008 Http://electrochem.xmu.edu.cn

Efficient Interface Enabled by Nano-Hydroxyapatite@Porous Carbon for Lithium-Sulfur Batteries

Jia-Yu Wang[1], Xue-Feng Tong[1], Qi-Fan Peng[1], Yue-Peng Guan[2*], Wei-Kun Wang[3], An-Bang Wang[3], Nai-Qiang Liu[4*], Ya-Qin Huang[1*]

(*1. Beijing Key Laboratory of Electrochemical Process and Technology for Materials, Key Laboratory of Biomedical Materials of Natural Macromolecules, Ministry of Education, Beijing University of Chemical Technology, Beijing 100029, P.R. China; 2. Beijing Key Laboratory of Clothing Materials R&D and Assessment, Beijing Engineering Research Center of Textile Nano Fiber, Beijing Institute of Fashion Technology, Beijing 100029, People's Republic of China; 3. Research Institute of Chemical Defense, Beijing 100191, P.R. China; 4. School of Materials Science and Engineering, Sichuan University of Science & Engineering, Zigong 643000, P.R. China*)

Abstract: The dissolution and "shuttle effect" of lithium polysulfides (LiPSs) hinder the application of lithium-sulfur (Li-S) batteries. To solve those problems, inspired by natural materials, a nano-hydroxyapatite@porous carbon derived from chicken cartilage (nano-HA@CCPC) was fabricated by employing a simple pre-carbonization and carbonization method, and applied in Li-S batteries. The nano-HA@CCPC would provide a reactive interface that allows efficient LiPSs reduction. With a strong affinity for LiPSs and an excellent electronic conductive path for converting LiPSs, the shuttle effect of LiPSs was confined and the redox kinetics of LiPSs was substantially enhanced. Li-S batteries employing nano-HA@CCPC-modified separators exhibited long cycle life and improved rate capability. At 0.5 C after 325 cycles, a specific capacity of 815 mAh·g^{-1} and a low capacity fading rate of 0.051% were obtained. The superior properties, sustainable raw materials, and facile preparation process make nano-HA@CCPC a promising additive material for practical Li-S batteries.

Key words: conductive carbon framework; nano-hydroxyapatite; reactive interface; modified separator; redox reaction kinetics; lithium-sulfur batteries

1 Introduction

Since a continuously mounting increasing demand for energy is depleting the stock of limited fossil fuel resources, lithium ion batteries (LIBs), the most representative recharge batteries, have been striding into daily life. The soaring demand for large-scale and high-energy storage systems, such as electric vehicles, has necessitated the development of batteries with capacitie s greater than those achievable with LIBs[1-3]. Therefore, to satisfy this demand, new-generation energy storage systems arise in this historic moment. The Li-S battery, one of the post-LIBs[4, 5], is considered a promising alternative on account of its high energy density (2600 Wh·kg^{-1}), high theoretical specific capacity (1675 mAh·g^{-1}), nontoxicity, and resource abundance[6-9]. However, the notorious "shuttle effect", which is responsible for the substantial capacity fade of Li-S batteries, poses an enormous

Cite as: Wang J Y, Tong X F, Peng Q F, Guan Y P, Wang W K, Wang A B, Liu N Q, Huang Y Q. Efficient interface enabled by nano-hydroxyapatite@porous carbon for lithium-sulfur batteries. *J. Electrochem.*, 2022, 28(11): 2219008.

Received: 2022-09-21, Revised: 2022-11-04. *Corresponding authors, Ya-Qin Huang: Tel: (86-10)64438266, huangyq@mail.buct.edu.cn, Yue-Peng Guan, 20210007@bift.edu.cn, Nai-Qiang Liu, liunaiqiang@suse.edu.cn.

challenge[10, 11].

Recently, extensive researches have focused on inhibiting the "shuttle effect" and increasing sulfur utilization[12-14]. Moreover, to effectively block lithium polysulfides (LiPSs), various carbon materials[15-18] have been applied to be a common strategy. These materials form a conductive network while limiting the formation of high-order LiPSs in pores, thereby enabling Li-S batteries to offer new opportunities for developing energy storage systems. However, nonpolar materials offer weak physical adsorption to polar LiPSs, resulting in such materials failing to restrain the shuttle of LiPSs during extended cycling. Thus, polar materials with strong affinity to LiPSs, such as TiO_2[19], MgO[20], Cr_2O_3[21], MnO_2[22] and heteroatom (N, S, and O, etc.) doped carbon[23], have been applied to inhibit the shuttle of LiPSs and considerably increase the utilization of sulfide by forming chemical bonds with LiPSs. However, the poor conductivity of metal oxides impedes their ability to continue the conversion of adsorbed LiPSs. Therefore, metal sulfides, nitrides and phosphides (such as CoS_2[24], MoS_2[25, 26], NiCoP[27] and TiN[28]) with high conductivity have been investigated, which could potentially reduce polarization, and increase the capacity and operating life of batteries. To better limit the dissolution of polysulfides, considerable attention is being devoted to constructing an effective electrode interface with newly developed electrode materials to meet the multi-functional requirements of Li-S batteries. To regulate the electrochemical redox reactions of LiPSs intermediates, Zhang et al. constructed multifunctional triple-phase interfaces using well-distributed $CoSe_2$ nanodots on a graphene matrix ($CoSe_2$/G)[29]. Zhao et al. fabricated refined interfaces by using two nanotube paper (CNTp) interlayers, which could facilitate the formation of uniform charge transfer and ion flue[30]. Li et al. constructed Co/N-codoped carbon of corrugated 2D morphology, enabling LiPSs affinity and abundant electrolyte/electrode interfaces[31]. These studies inspired us to explore the aforementioned processes in more depth.

The conversion of sulfur species in batteries is strongly dependent on the physicochemical properties of interfaces. Note that it is critical to developing a high-efficiency reactive interface that satisfies the following requirements: (1) a high affinity between the interface and LiPSs, which is essential to immobilize LiPSs and improve charge transfer, (2) high ion transport at the interface, and (3) exceptionally stable interfaces between phases.

In our previous work, we determined that nonconductive nano-hydroxyapatite (nano-HA) exhibits significant adsorption of LiPSs[32]. However, the performance of sulfur cells with nano-HA as an additive is limited by its non-conductive nature. Conductive carbon frameworks, which provides both high electronic conductivity and pore structure for ion transportation, are promising materials to construct efficient sulfur reaction interfaces with nano-HA. Animal cartilages could be encouraging precursors for constructing an efficient reactive interface of nano-HA and porous carbon for Li-S batteries (Figure 1a and 1b). They are natural organic/inorganic composite materials that primarily comprise structural collagen grid and a certain amount of hydroxyapatite (HA). In general, during the carbonization process, HA serves as an *in-situ* self-sacrificial template to fabricate the porous framework in animal bones[33]. The content of HA is a key indicator. Excessive HA content may lead to a disconnected carbon network of the product. Among the animal cartilages, chicken cartilage provides suitable HA content.

The lower HA content in chicken cartilage than that in hard bone is beneficial to obtaining high carbon yield and forming a conductive framework for improving charge transfer, and during the carbonization process of chicken cartilage, orderly distributed HA maintains its nanoscale properties and *in-situ* embeds in the porous carbon to form carbon-coated nano-HA structures, enhancing the affinity for adsorbing LiPSs.

Here, we selected chicken cartilage as a precursor to construct a nano-hydroxyapatite@chicken cartilage porous carbon (nano-HA@CCPC) reactive interface for advanced Li-S batteries. With the suitable HA

content, a uniform interface was constructed which allows efficient sulfur reduction. During the carbonization process, the orderly distributed HA maintained its nanoscale properties and in-situ embedded in the porous carbon to form carbon-coated nano-HA structures. The nano-HA@CCPC showed high absorption and catalytic capability, and thus, Li-S batteries with the nano-HA@CCPC-modified separator exhibited superior specific capacity, rate performance, and especially long-term cycling stability. After 325 cycles at 0.5 C, these batteries showed a specific capacity of 815 mAh·g^{-1} and the loss of capacity per cycle was as low as 0.051%. The nano-HA@CCPC is a promising material for advancing the adoption of LiPSs.

2 Experimental

2.1 Preparation of Nano-HA@CCPC

Raw chicken cartilage was dried and ground to a powder before carbonization, and then the chicken cartilage was pre-carbonized at 400 ℃ with a heating rate of 5 ℃·min^{-1} in a tube furnace (CNT Furnace ZSK1200) under a N_2 atmosphere for 2 h. The resultant chicken carbon precursor and KOH were mixed (mass ratio 1:1) and heated to 800 ℃ at 5 ℃·min^{-1} under a N_2 atmosphere. After cooling, the obtained carbon material was washed multiple times with distilled water until the residual KOH was removed. It was then dried at 60 ℃ for 24 h to obtain the nano-HA@CCPC composite. As a control sample, the nano-HA was prepared by re-calcining the nano-HA@CCPC composite in an air under the same calcining conditions and then the chicken cartilage based porous carbon (CCPC) was prepared by successively washing nano-HA@CCPC with 1.5 mol hydrochloric acid and distilled water until the nano-HA was completely removed.

2.2 Preparation of the Nano-HA@CCPC-Modified Separator

To obtain the nano-HA@CCPC modified separator, a mixture of 45wt% nano-HA@CCPC powder, 45wt% acetylene black (AB), and 10wt% LA132 were prepared as a slurry and directly coated onto a polypropylene (PP) separator. The coated separator was then dried in a vacuum oven at 60 ℃ for 24 h before being cut into circular disks (19 mm diameter). The control samples (nano-HA- and CCPC-modified separators) were prepared by using the same method.

2.3 Preparation of the Li_2S_6 Solution

Li_2S_6 solution was used to investigate the adsorption of LiPSs according to a previously reported method[34]. In particular, sublimed sulfur and Li_2S were mixed (molar ratio 5:1) with 1,3-dioxolane (DOL) and 1,2-dimethoxyethane (DME) (volume ratio 1:1) under an argon atmosphere and the resultant solution was placed to stand for 2 days to form Li_2S_6.

2.4 Assembly of Li_2S_6 Symmetric Battery

The Li_2S_6 symmetric batteries were assembled by using identical electrodes as the cathode and anode simultaneously. To prepare the nano-HA@CCPC-modified electrodes, 45wt% nano-HA@CCPC powder, 45wt% AB, and 10wt% LA132 were mixed into a homogeneous slurry, and directly coated on aluminum foil. As a control sample, the nano-HA and CCPC electrode was prepared with the same procedure. And the AB electrode was prepared by mixing AB with LA132 (mass ratio 9:1). The electrodes were obtained after the coated foils were cut into 12.0 mm disks. The batteries were then assembled into CR2025 coin cells with two identical electrodes, Celgard 2325 separator and 40 μL Li_2S_6 electrolyte. The Li_2S_6 electrolyte (0.05 mol·L^{-1}) was prepared by adding sulfur and Li_2S (molar ratio 5:1) in a mixture of DOL and DME (volume ratio 1:1) containing 1 mol·L^{-1} lithium bis(trifluoromethanesulfonyl) imide (LITFSI) and 0.4 mol·L^{-1} $LiNO_3$ under continuous magnetic stirring.

2.5 Battery Assembly and Material Characterization

In this study, 63wt% sublimed sulfur, 30wt% AB, and 7wt% LA132 were mixed into a homogeneous slurry and directly coated onto aluminum foil, obtaining the sulfur electrodes with a sulfur loading of 1.0 ~ 1.3 mg·cm^{-2}. The counter electrode was a foil of Li metal, and the electrolyte was formed by dissolving 1 mol·L^{-1} LITFSI and 0.4 mol·L^{-1} $LiNO_3$ in a combination of DOL and DME (volume ratio 1:1). The nano-

HA-, CCPC-, and nano-HA@CC PC-modified separators were adopted as the separators with the coated side facing the cathode in the coin cells. The CR2025 coin cells were then assembled in an argon-filled glove box.

Energy dispersive spectroscope (EDS, Quanta 650, FEI) and scanning electron microscope (SEM, JSM-7500F, JEOL) were used to characterize the surface morphology of and elemental distribution in the nano-HA@CCPC. The elemental composition of the nano-HA@CCPC and the chemical adsorption characteristics of the nano-HA@CCPC/Li_2S_6 composite were investigated with X-ray photoelectron spectroscopy (XPS). The Brunauer-Emmett-Teller (BET) data were calculated from ASAP 2020 V4.01. The compositions of the raw chicken cartilage and nano-HA@CCPC were characterized by thermogravimetric analyzer (TGA, Hengjiu, China). X-ray diffraction (XRD) patterns were obtained by a D/max 2500 V X-ray diffractometer, and the adsorption of LiPSs onto the samples was studied using UV-vis spectroscope (TU-1810). In the voltage window from 1.7 to 2.8 V vs. Li/Li^+, a LAND-CT2001A instrument was used to measure the cycle performance. Electrochemical impedance spectroscopy (EIS) and cyclic voltammetry (CV) were then employed to perform measurements by using an Autolab PGSTAT204 in the frequency range from 100 mHz to 100 kHz and in the voltage window from 1.7 to 2.8 V with a sweep rate of 0.1 $mV \cdot s^{-1}$, respectively.

3 Results and Discussion

The synthesis of nano-HA@CCPC is illustrated in Figure 1a. In brief, the evenly grounded chicken cartilage was first carbonized in an air atmosphere. And according to TG curve (FigureS1 a), 400 ℃ could ensure maintenance of structure and limited loss of carbon source at the same time. The mixture of resultant chicken carbon precursor and KOH was heated to 800 ℃, after cooling and removing KOH, the nano-HA@CCPC composite was obtained. The XRD pattern of nano-HA@CCPC (Figure 1c) shows the coincident broad diffraction peaks at 23° and 43°, which correspond to the (002) and (100) lattice planes of graphite, respectively[35], indicating the amorphous structure. However, the diffraction peaks of HA crystal in the nano-HA@CCPC are not obvious which could be attributed to the coverage of amorphous carbon. Hence, to confirm the formation of HA, we calcined the nano-HA@CCPC in an air to remove carbon and the sample is denoted as nano-HA. The XRD pattern of nano-HA exhibits typical HA diffraction peaks, confirming the good crystallization of nano-HA particles[36-38]. In addition, to illuminate the interaction at the interface between nano-HA and CCPC, CCPC was prepared by removing nano-HA and TG curve confirms the complete removal of HA in CCPC. CCPC shows similar XRD patterns to nano-HA@CCPC.

The SEM image of nano-HA@CCPC along with the EDS mapping is shown in Figure 1d. The nano-HA@CCPC demonstrates a hierarchical porous structure with uniformly distributed N and Ca elements. This indicates the even distribution of HA on the carbon framework. And according to the SEM image of re-calcined nano HA particles (Figure S3a-b), the average particle size of HA is less than 100 nm. The reason for the distribution distinction of HA between the two materials could be attributed to the *in-situ*-covered carbon framework on the surface of HA, which limits the agglomeration of HA particles and results in small HA particles. Table S2 shows the atomic percentages. The Ca/P atomic ratio in the nano-HA@CCPC was 1.52, which is lesser than the theoretical value of HA crystal. It might be that the P-containing organic matter in the chicken cartilage led to P-rich porous carbon after carbonization, and the abundant P doping could improve the adsorption of LiPSs[39]. Besides, certain N atoms from organic matter (e.g., amino acids) would be doped into the carbon framework, enhancing the affinity of the nano-HA@CCPC toward LiPSs.

We explored pore structures of nano-HA@CCPC and nano-HA, with N_2 adsorption-desorption isotherms (Figure 1e). The formation of the pore structures is related to the carbonization process. KOH was adopted to activate the carbon by etching its surface. A

series of reactions occurred between the KOH and carbon (i.e., KOH → K_2O + H_2O, C + H_2O → H_2 + CO, CO + H_2O → H_2 + CO_2, K_2O + CO_2 → K_2CO_3, K_2O + H_2 → 2K + H_2O and K_2O + C → 2K + CO), and the produced CO_2, K_2O and K_2CO_3 are conducive of pore construction[40]. According to the IUPAC classification, the BET data of the nano-HA@CCPC exhibits the type I curve. With micropore filling in the low-relative-pressure region, a rapid increase in gas adsorption was induced[41], indicating a well-developed microporous structure of the nano-HA@CCPC. However, the low- and medium-pressure zones of nano-HA were highly coincident and the N_2 adsorption amount approached zero. Only certain adsorption occurred in the high-pressure zone, suggesting the macroporous structure of nano-HA material[42]. As shown in Figure 1f, the pore size distribution was further confirmed by density function theory (DFT) modeling. The nano-HA@CCPC shows a pore distribution primarily in the micropore and smaller in the mesopore regions, and the pore diameter is less than 4 nm. On the contrary, the nano-HA shows pore distribution in the mesopore and macropore regions. Table S1 summarizes the BET data of both

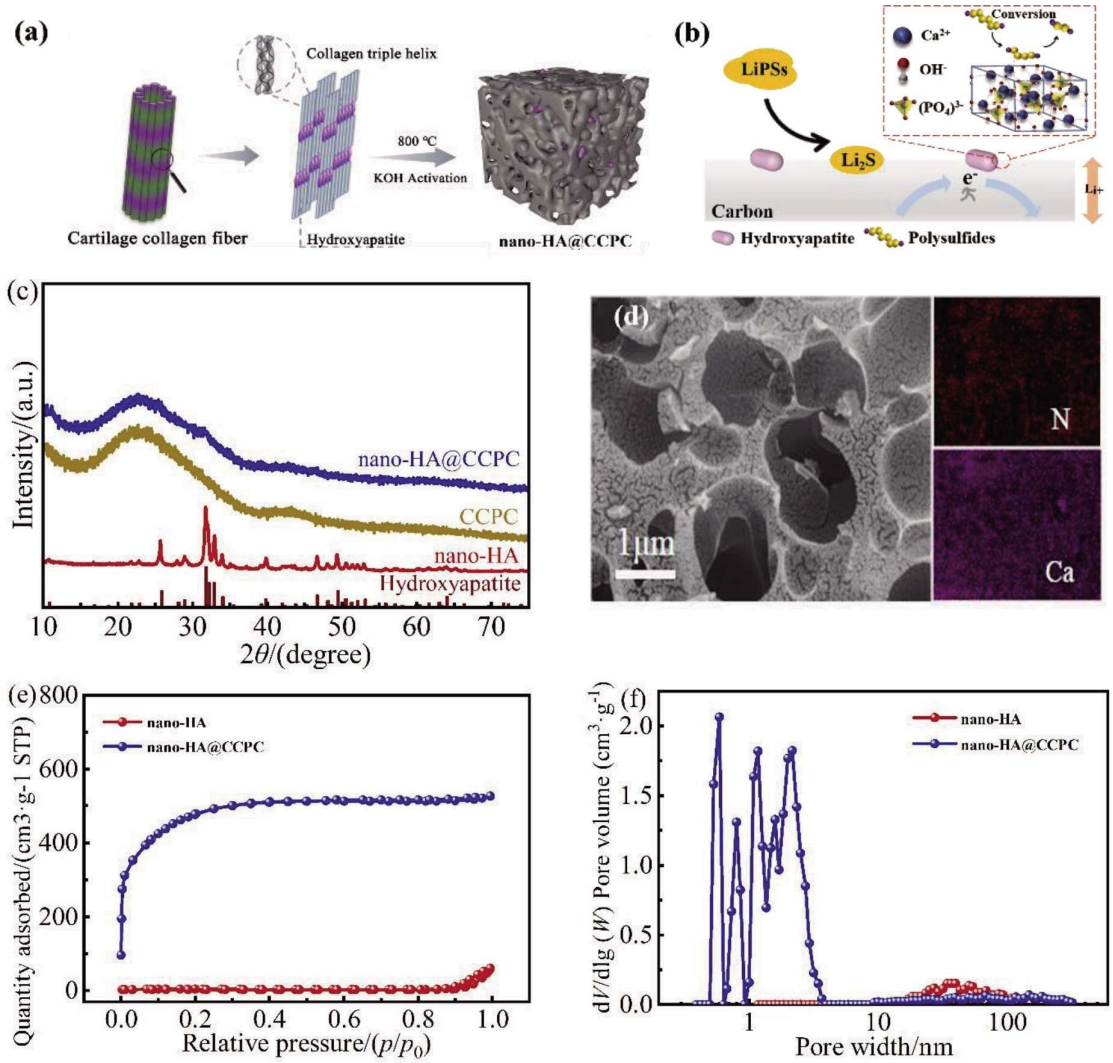

Figure 1 (a) Schematic diagram for the preparation procedure of nano-HA@CCPC. (b) Schematic illustration of the discharge process and nano-HA@CCPC incorporated carbon where LiPSs reduction is accelerated. (c) XRD patterns of the nano-HA, CCPC and nano-HA@CCPC. (d) SEM image for the nano-HA@CCPC and the corresponding EDS mapping images of N (red) and Ca (purple). (e) N_2 absorption-desorption isotherms and (f) pore diameter distribution curves for nano-HA and nano-HA@CCPC. (color on line)

nanoHA@CCPC and nano-HA. For the nano-HA@CCPC, a total specific surface area (SSA) of 2060.6 $m^2 \cdot g^{-1}$ with a micropore SSA of 498.0 $m^2 \cdot g^{-1}$ and an average pore size of 2.0 nm was obtained. The highly developed micro/mesoporous structure of the nano-HA@ CCPC might offer an interface with a larger surface area, thereby increasing the contact area between different phases and facilitating electrolyte penetration, which is beneficial for the fast transport of Li^+ ions[43].

The adsorption and catalytic capability of nano-HA@CCPC were further investigated. The UV-vis spectra of LiPSs before and after being mixed with various adsorbents are shown in Figure 2a. UV-vis spectrum of prepared LiPSs shows high absorption signal below 500 nm[44]. The signal is obviously reduced after being mixed with CCPC. This is related to the large specific surface area and rich pore structure of CCPC which lead to strong physical adsorption of LiPSs. The nano-HA@CCPC sample shows slightly higher absorption capacity of LiPSs compared to that of CCPC which is attributed to the chemical adsorption of LiPSs on nano-HA. XPS analysis was further conducted to understand the process of LiPSs adsorption onto nano-HA@CCPC. The XPS Ca 2p spectrum shows two peaks at binding energies of 351.19 ($2p_{1/2}$) and 347.69 eV ($2p_{3/2}$) (Figure 2b), which are consistent with those of Ca^{2+}[45]. After nano-HA@CCPC adsorbed Li_2S_6, the binding energies of the Ca 2p spectrum shifted toward lower binding energies at about 0.21 eV, indicating electron donation from sulfide to Ca^{2+}. This result demonstrates that Ca atoms in nano-HA@CCPC are effective for bonding S atoms in LiPSs[40]. Moreover, the P element plays an important role in nano-HA@CCPC, and the XPS P 2p spectrum shows two peaks at binding energies of 133.24 and 134.11 eV (PO_4^{3-}) (Figure 2c)[46-49]. After LiPSs adsorption, new peaks of the P 2p spectrum at 133.50 and 134.37 eV appeared, which corresponds to the interaction of P-S[50]. And the S 2p spectrum of the nano-HA@CCPC (Figure 2d) confirms these results. The S 2p spectrum shows four peaks, at 163.26 and 164.42 eV, corresponding to S-S/S-C, while at 168.56 and 169.82 eV, corresponding to sulfate species formed by the oxidation of sulfur in an air[51-53]. After the nano-HA@CCPC adsorbed Li_2S_6, two new peaks of the S 2p spectrum occurred at 163.73 and 164.89 eV, which can be attributed to S-P[54, 55].

Due to the strong P-S bond, the nano-HA exhibits good catalytic capability for LiPSs reduction. Both CV and EIS tests were carried out to gain insight into the role of the reactive interface in accelerating the LiPSs reduction reactions. The redox reactions kinetics were investigated by using Li_2S_6-electrolyte symmetric batteries with CV scan rate of 50 $mV \cdot s^{-1}$ and voltage window from -0.7 to 0.7 V (Figure 2e). The polarization profiles comprise the main redox current density of Li_2S_6 and the minor capacitive current density of free Li_2S_6[55]. The symmetric battery with nano-HA@CCPC exhibits twice current density as high as that of CCPC, indicating that more than simply enhancing the LiPSs adsorption, the introduction of nano-HA@CCPC also enhanced the redox reaction kinetics of LiPSs. The EIS profile shows the minimum charge-transfer resistance of the nano-HA@CCPC, further demonstrating that the high-efficiency reactive interface of nano-HA@CCPC enhances the reaction kinetics of LiPSs (Figure 2f)[56].

The original combining of the high LiPSs adsorption CCPC and nano-HA catalyst makes nano-HA@CCPC a promising candidate for Li-S batteries. The strong adsorption capacity constructs a micro-environment with higher LiPSs concentration around the nano-HA coated by CCPC, which is more beneficial to the transformation of LiPSs by HA catalysis. These results illustrate that the active interface of nano-HA@CCPC is highly affinitive to soluble LiPSs.

To illustrate the advantages of the nano-HA@CCPC-modified separator, we characterized the morphologies of the different modified separators using SEM (Figure 3a, Figure S4a and Figure S4b). The three separators show loose structure with numerous micro-sized voids and channels, facilitating electrolyte infiltration and Li^+ ion transport, and enables accommodation of the LiPSs. Cross-sectional SEM observation (Figure 3b) of the nano-HA@CCPC-

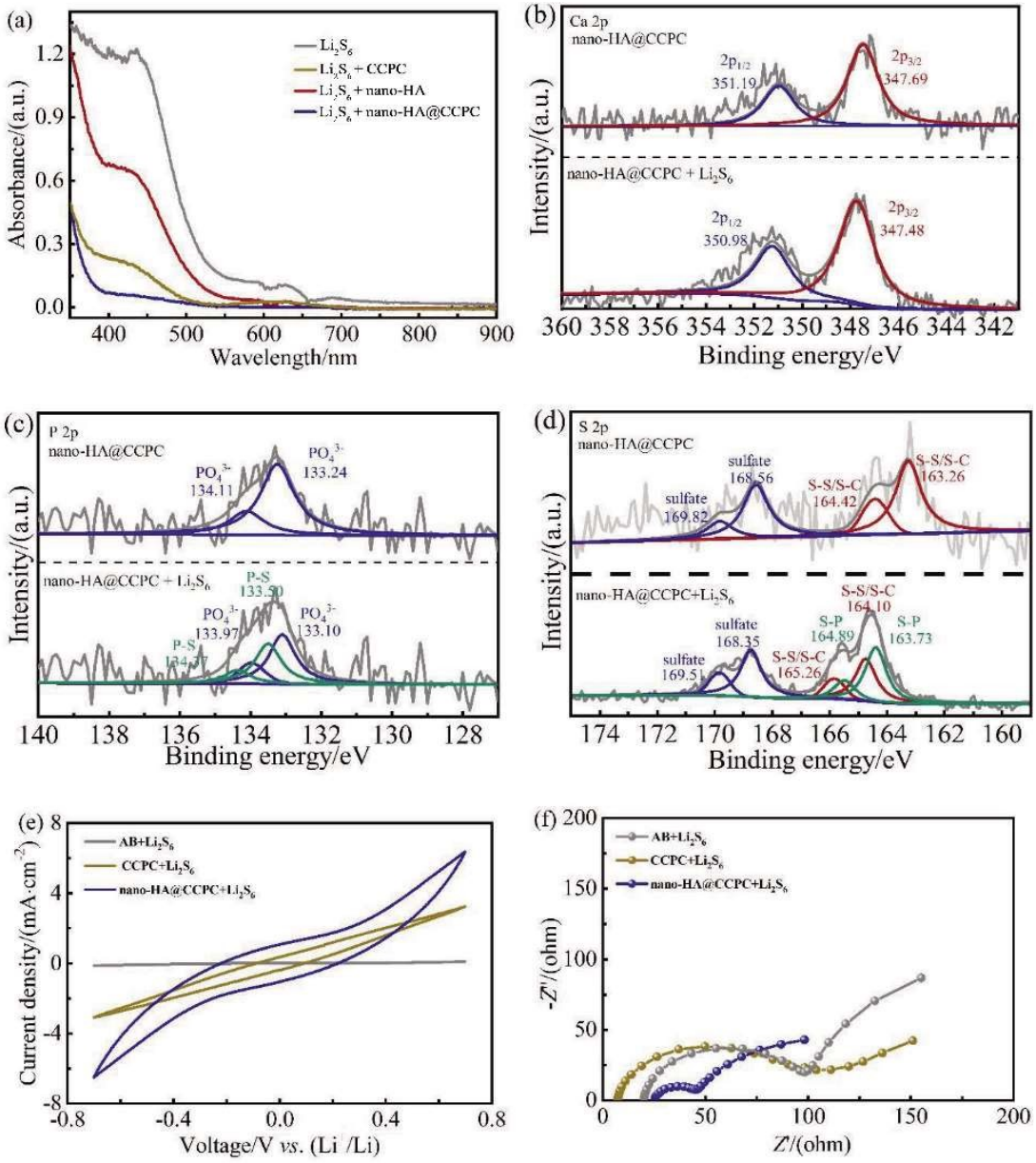

Figure 2 (a) UV-vis spectra of the Li_2S_6-containing solutions adding nano-HA, CCPC, and nano-HA@CCPC powders. (b-d) XPS spectra of the Ca 2p, P 2p and S 2p peaks of the nano-HA@CCPC and nano-HA@CCPC/Li_2S_6, together with their respective fitted peaks. (e) CV curves of symmetric cells to evaluate the conversion between soluble LiPSs. (f) EIS spectra of AB, CCPC, and nano-HA@CCPC in symmetric cells. (color on line)

modified separator demonstrates that the coating thickness is about 6 μm with the coated loading of only 0.07 mg·cm^{-2}. After folding, the undamaged nano-HA@CCPC-modified separator (Figure S5) retained its mechanical stability. Contact angle measurements were further implemented on different separators (Figure 3c-d, Figure S4c, and Figure S4d). Compared with the large contact angle of PP separator, both CCPC and nano-HA@CCPC-modified separators were completely wetted with water, signifying good electrolyte penetration. The nano-HA-modified separator exhibits a larger water contact angle, indicating that CCPC plays an excellent cooperative role with nano-HA in ion diffusion.

Moreover, we evaluated the electrochemical performance of Li-S batteries with CCPC-, and nano-

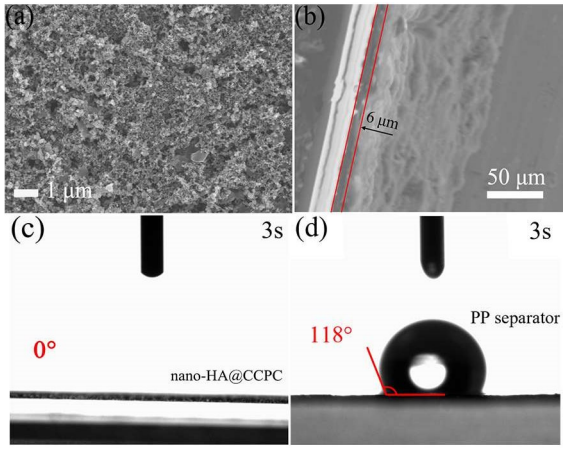

Figure 3 Characterization of the nano-HA@CCPC-modified separator. The surface (a) and cross-section (b) SEM images of the nano-HA@CCPC-modified separator. The contact angles for (c) nano-HA@CCPC-modified separator and (d) PP separator. (color on line)

HA@CCPC-modified separators (Figure 4). CV was conducted to illustrate the improved redox reactions of the Li-S batteries with the nano-HA@CCPC-modified separator (Figure 4a). The battery with the nano-HA@CCPC-modified separator exhibits sharp cathodic and anodic peaks. It shows a small polarization and a large current density compared with those of the CCPC-modified separator, indicating a faster reaction kinetics. These results suggest that the nano-HA@CCPC-modified separator constructs a conductive carbon framework, offering a high-efficiency interface to accelerate the conversion of LiPSs[32]. The galvanostatic discharge/charge voltage profiles of batteries with the separators at 0.5 C offer consistent results with CV. The voltage profiles show a classic two-step S redox process (Figure 4b-c). The high discharge plateau at 2.2 ~ 2.4 V is where S_8 converses to Li_2S_n ($4 \leqslant n \leqslant 8$), and the low one at 2.0 ~ 2.1 V represents the formation of Li_2S_2/Li_2S. All these plateaus are attributable to the reduction processes of S. The two plateaus at 2.27 and 2.38 V in the charge profiles represent the conversion of Li_2S_2/Li_2S to S_8/Li_2S_8, which corresponds to the oxidation processes of S[57, 58]. The battery with the nano-HA@CCPC-modified separator exhibits longer second plateaus and lower polarization (ΔE) than the batteries with CCPC- and nano-HA-modified separators (Figure S8), which could be attribute to the promoted LiPSs reduction. As the cycle number increased, the voltage curves of the battery with the nano-HA@CCPC-modified separator overlap well compared with those of the batteries with nano-HA- and CCPC-modified separators. These results indicate that the battery with the nano-HA@CCPC-modified separator exhibited good cycling stability. The cycling performance further confirms the above results. As shown in Figure 4d, all batteries were pre-activated for two cycles at 0.05 C. After 325 cycles, the batteries with the nano-HA@CCPC-modified separator retained a high capacity of 815 mAh·g^{-1}; the capacity fade after each cycle was 0.051%, and the Coulombic efficiency remained stable at ~99%. However, after 200 cycles, the batteries with the CCPC-modified separator displayed relatively low capacity of 700 mAh·g^{-1}. It is worth noting that after 20 cycles, the nano-HA@CCPC-modified separator still maintained a uniformly distributed surface morphology without obvious cracks (Figure S6). According to Equation 3-1, the shuttle factors of the batteries with the nano-HA@CCPC- and CCPC-modified separators at 0.5 C were 0.007 and 0.029, respectively, where C_{eff} is Coulombic efficiency and f is the shuttle factor. Figure S7b)[59].

Equation 3-1: $$C_{\text{eff}} = \frac{2f + \ln(1+f)}{2f - \ln(1-f)}$$

Consequently, the nano-HA@CCPC-modified separator effectively hinders the shuttle effect. The rate performance of batteries was investigated by cycling at rates of 0.2, 0.5, 1.0 and 2.0 C (Figure 4e). The battery with the nano-HA@CCPC-modified separator displayed reversible capacities of 1041, 916, 840, and 718 mAh·g^{-1} at 0.2, 0.5, 1.0 and 2.0 C, respectively. The specific capacities are higher than those of the batteries with CCPC-modified separators, which delivered capacities of 934, 754, 636, and 523 mAh·g^{-1}, respectively. When the rate was returned to 0.2 C, the battery with the nano-HA@CCPC-modified separator regained approximately 91% of its original capacity because of good electronic conductivity and fast reaction kinetics.

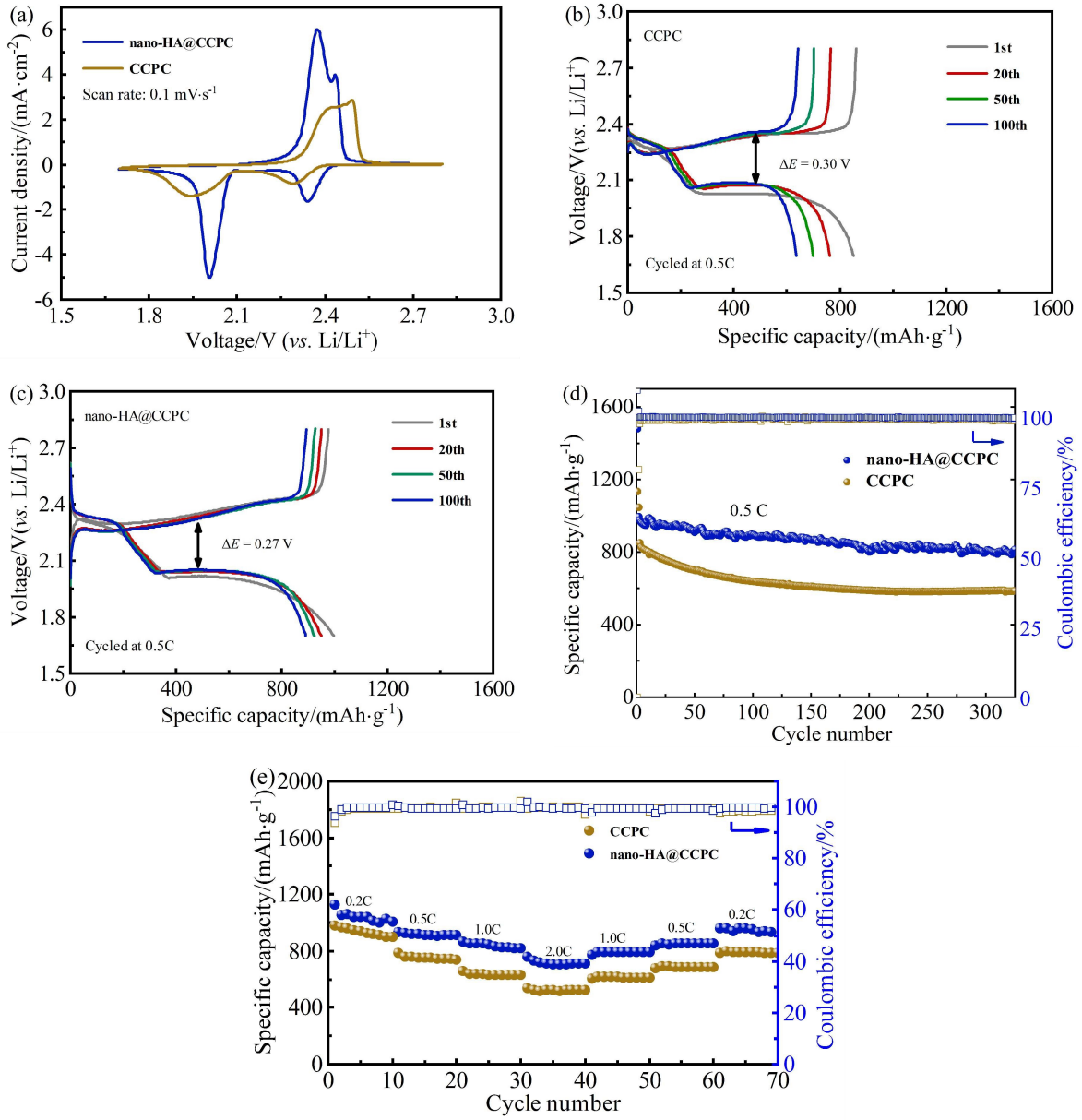

Figure 4 Electrochemical performance of Li-S batteries with different separators. (a) CV curves for Li-S batteries with CCPC or nano-HA@CCPC-modified separator. The galvanostatic discharge/charge voltage profiles of different cycles at 0.5 C for batteries with (b) CCPC- and (c) nano-HA@CCPC-modified separators, (d) the long-term cycling performance of batteries at 0.5 C, and (e) rate performance of batteries. (color on line)

These results demonstrate that the nano-HA@CCPC could construct a high-efficiency reactive interface by providing sufficient active sites of LiPSs adsorption and effectively accelerate the conversion of LiPSs. Furthermore, the Li-S batteries with the nano-HA@CCPC-modified separator exhibited advantages in cycling performance compared with batteries in previously reported works (Table S4). To further demonstrate the kinetics of LiPSs reduction reactions, the onset potential of the second step of the Li-S reduction reaction is defined as the current density of 10 μA·cm^{-2} beyond the baseline current (Figure S9). The battery with nano-HA@CCPC-modified separator exhibits the smallest onset potential of the second cathodic peak, illustrating that the liquid-liquid reaction can proceed with the minimum

required driving force and that the nano-HA@CCPC has a certain catalytic effect[60]. Therefore, the redox reaction kinetics of battery with the nano-HA@CCPC-modified separator are strongly enhanced.

4 Conclusions

In conclusion, we constructed an efficient reactive interface by using nano-HA@CCPC to regulate the electrochemical redox reaction of LiPSs. The rich interface area and excellent electronic conductive path effectively accelerated the LiPSs conversion. In particular, the good dispersion and embedment of nano-HA into the porous carbon enhanced the affinity of the interface for LiPSs. Furthermore, the CCPC conductive framework played an excellent cooperative role with nano-HA in the redox reaction kinetics of LiPSs. The batteries employing the nano-HA@CCPC-modified separators displayed high capacity, good rate performance, long cycle life, and good stability. When cycled at 0.5 C for 325 cycles, the batteries still displayed a specific capacity of 815 $mAh \cdot g^{-1}$ with an average capacity fading rate of only 0.051% per cycle. Because of sufficient sources, facile preparation method, and excellent electrochemical performance, nano-HA@CCPC is a promising additive for Li-S battery applications.

Declarations of Interest

The authors declare that there is no conflict of interests regarding the publication of this article.

Acknowledgments

This work was supported by the National Natural Science Foundation of China.

No. 51861165101

Foundation name: Multi-functional ion-exchange membrane for sulfur-based batteries and understanding the charge transport and ion-immobilization mechanism

References:

[1] Goodenough J B, Park K S. The Li-ion rechargeable battery: a perspective [J]. J. Am. Chem. Soc., 2013, 135(4): 1167-1176.

[2] Manthiram A, Fu Y, Chung S H, Zu C, Su Y S. Rechargeable lithium-sulfur batteries[J]. Chem. Rev., 2014, 114(23): 11751-11787.

[3] Sun Y M, Liu N A, Cui Y. Promises and challenges of nanomaterials for lithium-based rechargeable batteries [J]. Nat. Energy, 2016, 1(7): 16071.

[4] Marom R, Amalraj S F, Leifer N, Jacob D, Aurbach D. A review of advanced and practical lithium battery materials [J]. J. Mater. Chem., 2011, 21(27): 9938-9954.

[5] Girishkumar G, Mccloskey B, Luntz A C, Swanson S, Wilcke W. Lithium-air battery: promise and challenges[J]. J. Phys. Chem. Lett., 2010, 1(14): 2193-2203.

[6] Rosenman A, Markevich E, Salitra G, Aurbach D, Garsuch A, Chesneau F F. Review on Li-sulfur battery systems: an integral perspective[J]. Adv. Energy Mater., 2015, 5(16): 1500212.

[7] Peng H J, Huang J Q, Cheng X B, Zhang Q. Review on high-loading and high-energy lithium-sulfur batteries [J]. Adv. Energy Mater., 2017, 7(24): 1700260.

[8] Choi J W, Kim J K, Cheruvally G, Ahn J H, Ahn H J, Kim K W. Rechargeable lithium/sulfur battery with suitable mixed liquid electrolytes[J]. Electrochim. Acta, 2007, 52(5): 2075-2082.

[9] Yang Y, Zheng G Y, Cui Y. Nanostructured sulfur cathodes[J]. Chem. Soc. Rev., 2013, 44(24): 3018-3032.

[10] Zhang S S. Liquid electrolyte lithium/sulfur battery: fundamental chemistry, problems, and solutions[J]. J. Power Sources, 2013, 231(2): 153-162.

[11] Liu M, Li Q, Qin X Y, Liang G M, Han W J, Zhou D, He Y B, Li B H, Kang F Y. Suppressing self-discharge and shuttle effect of lithium-sulfur batteries with V_2O_5-decorated carbon nanofiber interlayer[J]. Small, 2017, 13(12): 1602539.

[12] Chung S H, Manthiram A. A polyethylene glycol-supported microporous carbon coating as a polysulfide trap for utilizing pure sulfur cathodes in lithium-sulfur batteries [J]. Adv. Mater., 2014, 26(43): 7352-7357.

[13] Huang J Q, Zhang Q, Peng H J, Liu X Y, Qian W Z, Wei F. Ionic shield for polysulfides towards highly-stable lithium-sulfur batteries[J]. Energy Environ. Sci., 2013, 7(1): 347-353.

[14] Liu D, Zhang C, Zhou G, Lv W, Ling G, Zhi L, Yang Q H. Catalytic effects in lithium-sulfur batteries: promoted sulfur transformation and reduced shuttle effect[J]. Adv. Sci., 2018, 5(1): 1700270.

[15] Wu H W, Ying H, Zhang W C, Sun X, Yang Y W, Wang L, Zong M. Lock of sulfur with carbon black and a

three-dimensional graphene@carbon nanotubes coated separator for lithium-sulfur batteries[J]. J. Alloys Compd., 2017, 708: 743-750.

[16] Xiao D J, Lu C X, Chen C M, Yuan S X. CeO_2-webbed carbon nanotubes as a highly efficient sulfur host for lithium-sulfur batteries[J]. Energy Storage Mater., 2018, 10: 216-222.

[17] Peng H J, Huang J Q, Zhao M Q, Zhang Q, Cheng X B, Liu X Y, Qian W Z, Wei F. Carbon: Nanoarchitectured graphene/CNT@porous carbon with extraordinary electrical conductivity and interconnected micro/mesopores for lithium-sulfur batteries[J]. Adv. Funct. Mater., 2014, 24(19): 2772-2781.

[18] Rui W, Chen S G, Deng J H, Xun H, Song Y J, Gan R Y, Wan X J, Wei Z D. Hierarchically porous nitrogen-doped carbon as cathode for lithium-sulfur batteries[J]. J. Energy Chem., 2018, 27: 1661-1667.

[19] Shao H Y, Wang W K, Zhang H, Wang A B, Chen X N, Huang Y Q. Nano-TiO_2 decorated carbon coating on the separator to physically and chemically suppress the shuttle effect for lithium-sulfur battery[J]. J. Power Sources, 2018, 378: 537-545.

[20] Zhao X Y, Wang J Y, Sun X G, Wei K R, Wang W K, Wang A B, Huang Y Q, Guan Y P. Hierarchical porous carbon with Nano-MgO as efficient sulfur species microreactors for lithium-sulfur battery[J]. J. Electrochem. Soc., 2021, 168(4): 040506.

[21] Guan Y P, Liu X J, Akhtar N, Wang A B, Wang W K, Zhang H, Suntivich J, Huang Y Q. Cr_2O_3 nanoparticle decorated carbon nanofibers derived from solid leather wastes for high performance lithium-sulfur battery separator coating[J]. J. Electrochem. Soc., 2019, 166(8): A1671.

[22] Kong W B, Yan L J, Luo Y F, Wang D T, Jiang K L, Li Q Q, Fan S S, Wang J P. Li-S batteries: Ultrathin MnO_2/graphene oxide/carbon nanotube interlayer as efficient polysulfide-trapping shield for high-performance Li&N dash; S batteries[J]. Adv. Funct. Mater., 2017, 27(18): 1606663.

[23] Sun Z H, Zhang J Q, Yin L C, Hu G J, Fang R P, Cheng H M, Li F. Conductive porous vanadium nitride/graphene composite as chemical anchor of polysulfides for lithium-sulfur batteries[J]. Nat. Commun., 2017, 8: 14627.

[24] Zeng P, Huang L W, Zhang X L, Han Y M, Chen Y G. Inhibiting polysulfides diffusion of lithium-sulfur batteries using an acetylene black-CoS_2 modified separator: mechanism research and performance improvement [J]. Appl. Surf. Sci., 2018, 427: 242-252.

[25] Xiang K X, Wen X Y, Hu J, Wang S C, Chen H. Rational fabrication of nitrogen and sulfur codoped carbon nanotubes/MoS_2 for high-performance lithium-sulfur batteries[J]. ChemSusChem, 2019, 12(15): 3602-3614.

[26] Zhou T H, Lv W, Li J, Zhou G M, Zhao Y, Fan S X, Liu B L, Li B H, Kang F Y, Yang Q H. Twinborn TiO_2-tin heterostructures enabling smooth trapping-diffusion-conversion of polysulfides towards ultralong life lithium-sulfur batteries[J]. Energy Environ. Sci., 2017, 10(7): 1694-1703.

[27] Yuan H, Peng H J, Li B Q, Xie J, Kong L, Zhao M, Chen X, Huang J Q, Zhang Q. Conductive and catalytic triple-phase interfaces enabling uniform nucleation in high-rate lithium-sulfur batteries[J]. Adv. Energy Mater., 2019, 9(1): 1802768.

[28] Peng Y Y, Wen Z P, Liu C Y, Zeng J, Wang Y H, Zhao J B. Refining interfaces between electrolyte and both electrodes with carbon nanotube paper for high-loading lithium-sulfur batteries[J]. ACS Appl. Mater. Interfaces, 2019, 11(7): 6986-6994.

[29] Liu N Q, Fei A, Wang W K, Shao H Y, Zhang H, Wang A B, Xu Z C, Huang Y Q. Nano-hydroxyapatite as an efficient polysulfide absorbent for high-performance Li-S batteries[J]. Electrochim. Acta, 2016, 215: 162-170.

[30] Garnero P. The role of collagen organization on the properties of bone[J]. Calcif. Tissue Int., 2015, 97(3): 229-240.

[31] Peng Q F, Yu F, Wang W K, Wang A B, Wang F, Huang Y Q. Ultralight polyethylenimine/porous carbon modified separator as an effective polysulfide-blocking barrier for lithium-sulfur battery[J]. Electrochim. Acta, 2019, 299: 749-755.

[32] Peng Q F, Fan Y, Huang B C, Huang Y Q. Carbon-containing bone hydroxyapatite obtained from tuna fish bone with high adsorption performance for congo red[J]. RSC Adv., 2017, 7(43): 26968-26973.

[33] Do V, Deepika, Kim M S, Kim M S, Lee K R, Cho W I. Carbon nitride phosphorus as an effective lithium polysulfide adsorbent for lithium-sulfur batteries[J]. ACS Appl. Mater. Interfaces, 2019, 11(12): 11431-11441.

[34] Shao H Y, Ai F, Wang W K, Zhang H, Wang A B, Wang F, Huang Y Q. Crab shell-derived nitrogen-doped micro-/mesoporous carbon as an effective separator coating for high energy lithium-sulfur batteries[J]. J. Mater. Chem. A, 2017, 5(37): 19892-19900.

[35] Zhang B, Qin X, Li G R, Gao X P. Enhancement of long stability of sulfur cathode by encapsulating sulfur into micropores of carbon spheres[J]. Energy Environ. Sci., 2010, 3(10): 1531-1537.

[36] Yamada H, Nakamura H, Nakahara F, Moriguchi I, Kudo

T. Electrochemical study of high electrochemical double layer capacitance of ordered porous carbons with both meso/macropores and micropores[J]. J. Phys. Chem. C, 2007, 111(1): 227-233.

[37] Peng H J, Zhang Z W, Huang J Q, Zhang G, Xie J, Xu W T, Shi J L, Chen X, Cheng X B, Zhang Q. A cooperative interface for highly efficient lithium-sulfur batteries [J]. Adv. Mater., 2016, 28(43): 9551-9558.

[38] Zou Q L, Lu Y C. Solvent-dictated lithium sulfur redox reactions: an operando UV-vis spectroscopic study [J]. J. Phys. Chem. Lett., 2016, 7(8): 1518-1525.

[39] Robinson L, Salma-Ancane K, Stipniece L, Meenan B J, Boyd A R. The deposition of strontium and zinc Co-substituted hydroxyapatite coatings[J]. J Mater. Sci. Mater. Med., 2017, 28(3): 51.

[40] Baradaran S, Nasiri-Tabrizi B, Shirazi F S, Saber-Samandari S, Shahtalebi S, Basirun W J. Wet chemistry approach to the preparation of tantalum-doped hydroxyapatite: dopant content effects[J]. Ceram. Int., 2018, 44(3): 2768-2781.

[41] Ma X L, Ning G Q, Qi C L, Xu C G, Gao J S. Phosphorus and nitrogen dual-doped few-layered porous graphene: A high-performance anode material for lithium-ion batteries [J]. ACS Appl. Mater. Interfaces, 2014, 6(16): 14415-14422.

[42] Guo M Q, Huang J Q, Kong X Y, Peng H J, Shui H, Qian F Y, Zhu L, Zhu W C, Zhang Q. Hydrothermal synthesis of porous phosphorus-doped carbon nanotubes and their use in the oxygen reduction reaction and lithium-sulfur batteries[J]. New Carbon Mater., 2016, 31(3): 352-362.

[43] Wu H L, Mou J R, Zhou L, Zheng Q J, Jiang N, Lin D M. Cloud cap-like, hierarchically porous carbon derived from mushroom as an excellent host cathode for high performance lithium-sulfur batteries[J]. Electrochim. Acta, 2016, 212: 1021-1030.

[44] Do V, Deepika, Kim M S, Kim MS, Lee K R, Cho W I. Carbon nitride phosphorus as an effective lithium polysulfide adsorbent for lithium-sulfur batteries[J]. ACS Appl. Mater. Interfaces, 2019, 11(12): 11431-11441.

[45] Yang J, Chen F, Li C, Bai T, Long B, Zhou X Y. A free-standing sulfur-doped microporous carbon interlayer derived from luffa sponge for high performance lithium-sulfur batteries[J]. J. Mater. Chem. A, 2016, 4(37): 14324-14333.

[46] Wu X H, Mirolo M, Vaz C A F, Novak P, El Kazzi M. Reactivity and potential profile across the electrochemical $LiCoO_2$-Li_3PS_4 interface probed by operando X-ray photoelectron spectroscopy[J]. ACS Appl. Mater. Interfaces, 2021, 13(36): 42670-42681.

[47] Luo C, Zhu Y J, Borodin O, Gao T, Fan X L, Xu Y H, Xu K, Wang C S. Activation of oxygen-stabilized sulfur for Li and Na batteries[J]. Adv. Funct. Mater., 2016, 26(5): 745-752.

[48] Liu X, Huang J Q, Zhang Q, Mai L Q. Nanostructured metal oxides and sulfides for lithium-sulfur batteries [J]. Adv. Mater., 2017, 29(20): 1601759.

[49] Mikhaylik Y V, Akridge J R. Polysulfide shuttle study in the Li/S battery system[J]. J. Electrochem. Soc., 2004, 151(11): A1969.

[50] Cheon S E, Ko K S, Cho J H, Kim S W, Chin E Y, Kim H T. Rechargeable lithium sulfur battery[J]. J. Electrochem. Soc., 2003, 150(6): A796.

[51] Huang J Q, Zhang Q, Zhang S M, Liu X F, Zhu W, Qian W Z, Wei F. Aligned sulfur-coated carbon nanotubes with a polyethylene glycol barrier at one end for use as a high efficiency sulfur cathode[J]. Carbon, 2013, 58: 99-106.

[52] Yuan Z, Peng H J, Hou T Z, Huang J Q, Chen C M, Wang D W, Cheng X B, Wei F, Zhang Q. Powering lithium-sulfur battery performance by propelling polysulfide redox at sulfiphilic hosts[J]. Nano Lett., 2016, 16(1): 519-527.

用纳米羟基磷灰石@多孔碳构建锂硫电池高效反应界面

汪佳裕[1],仝学锋[1],彭启繁[1],关越鹏[2*],王维坤[3],
王安邦[3],刘乃强[4*],黄雅钦[1*]

(1. 材料电化学过程与技术北京市重点实验室, 天然高分子生物医用材料教育部重点实验室, 北京化工大学, 北京 100029; 2. 北京服装学院服装材料研究开发与评价北京市重点实验室, 北京市纺织纳米纤维工程技术研究中心, 北京 100029; 3. 防化研究院, 北京 100191; 4. 四川轻化工大学材料科学与工程学院, 四川 自贡, 643000)

摘要: 由于正极活性物质硫具有能量密度高、成本低廉和储量丰富等优点,锂硫(Li-S)电池受到了人们的极大关注。然而,锂硫电池充放电过程中产生的多硫化锂的"穿梭效应"严重阻碍了其实用化进程。为了解决这个问题,本研究借助动物软骨的组成和结构特点,制备了纳米羟基磷灰石@多孔碳(nano-HA@CCPC)复合材料,并以此设计了面向正极的锂硫电池隔膜涂层。研究表明,纳米羟基磷灰石不仅对多硫化物具有吸附固定作用,并且对多硫化锂的转化具有催化作用,加快了多硫化锂的氧化还原动力学,有效地提升了活性物质硫的利用率。另外,软骨基碳复合材料的多孔结构形成了很好的导电网络,为电化学反应提供了优良的电子传导路径;也有利于电解液的浸润,加快了离子传输;碳的氮原子掺杂进一步限制了多硫化物的穿梭效应。因此,采用 nano-HA@CCPC 隔膜涂层的锂硫电池表现出较长的循环寿命、低的容量损失以及高的倍率性能。在 0.5 C 下,循环 325 次后,电池仍然能保持 815 mAh·g^{-1} 的放电比容量,并且每次的容量衰减率仅为 0.051%。nano-HA@CCPC 的设计制备将为锂硫电池的发展提供新材料。

关键词: 导电碳框架; 纳米羟基磷灰石; 反应界面; 改性隔膜; 氧化还原反应动力学; 锂硫电池